CrystEngComm

Accepted Manuscript

ROYAL SOCIETY OF CHEMISTRY

www.rsc.org/crystengcomm

Journal Name

RSCPublishing

ARTICLE

Synthesis of nickel hydroxychloride microspheres via a facile template-free process and their conversion to β-$Ni(OH)_2$ microspheres

Cite this: DOI: 10.1039/x0xx00000x

Received 00th January 2012,
Accepted 00th January 2012

DOI: 10.1039/x0xx00000x

www.rsc.org/

Kay He, Gaoling Zhao*, Gaorong Han

Hierarchical flower-like nickel hydroxychloride microspheres were prepared by forced hydrolysis reaction of nickel chloride hexahydrate in ethanol via a facile template-free solvothermal process. The flower-like nickel hydroxychloride microspheres, which were prepared with low concentration of Ni without adding H_2O, were composed of crumpled nanosheets with random orientation. The aggregation growth and dissolution-recrystallization process were involved in the formation of flower-like nickel hydroxychloride microspheres. The flower-like β-$Ni(OH)_2$ microspheres were prepared by nickel hydroxychloride microspheres treated with high concentration of KOH. The β-$Ni(OH)_2$ microspheres prepared with higher concentration of KOH showed better electrochemical performance, while the β-$Ni(OH)_2$ microspheres prepared with lower concentration of KOH showed better adsorption activity for acid fuchsine.

1. Introduction

Controlled morphologies of various nanostructures are of intense fundamental interests[1]. Great progresses have been made in the preparation of the nanostructures such as quantum dots, nanorods, nanowires, nanosheets, nanocubes, hierarchical structures, etc. The hierarchical flower-like structures take advantage of a tailored nano-design, controlled accessibility to the active sites, tunable pore size and volume, large number of pore openings and high surface area[2, 3]. However, researchers continue to face great challenges in the construction of well-defined hierarchical flower-like structures with complex morphologies.

Layered nickel hydroxy compounds, such as α-$Ni(OH)_2$, β-$Ni(OH)_2$ and hydroxy salts of nickel, are related to the brucite-like or brucite structure[4-6], which have attracted great attention for the applications such as high performance supercapacitors, water treatment, and lithium batteries[7] due to the interesting interlayer chemical properties. Nickel hydroxy compounds are prone to form flower-like structures because of the internal structures[8, 9], but in many cases, well-defined flower-like structures are hard to be formed in the absence of organic additives[10, 11]. The researchers usually employ organic additives to facilitate the formation of the flower-like structures[12]. In this process, the nickel precursor is modified by the complexation of organic additives, and the nucleation and growth processes are changed[13]. However, the post-synthetic treatments aimed to remove the organic additives might destroy the as-prepared products and increase costs. Ideally, a facile template-free process is preferred for preparing flower-like structures of nickel hydroxy compounds. In this sense, it is highly desirable to develop a suitable precursor which prefers to form flower-like structures spontaneously.

Herein, a facile template-free solvothermal process was used for the fabrication of hierarchical flower-like nickel hydroxychloride. The samples are prepared with nickel(II) chloride hexahydrate as Ni source and ethanol as solvent at 170 °C. Effects of various parameters, such as the reaction time and the concentration of Ni and adscititious H_2O, on the crystallinity and morphology of nickel hydroxychloride were investigated. The flower-like β-$Ni(OH)_2$ microspheres were prepared by nickel hydroxychloride microspheres treated with high concentration of KOH. The formation mechanisms of the flower-like nickel hydroxychloride microspheres and β-$Ni(OH)_2$ microspheres were proposed. The electrochemical performance and the adsorption activity of β-$Ni(OH)_2$ were also evaluated. To our knowledge, the flower-like nickel hydroxychloride is reported here for the first time and is used as a new precursor for β-$Ni(OH)_2$.

2. Experiment

2.1. Preparation

All the chemicals were of analytical grade and were used as received without further purification. In a typical experiment, nickel(II) chloride hexahydrate (1.08 g) was dissolved in ethanol (30.8 ml) to get a transparent green solution with 0.14 M Ni. The solution was sealed within a Teflon-lined autoclave (40 mL) which was filled about 80% of its capacity and then heated at 170 °C under a solvothermal condition for various time. The solid products were collected by centrifugation, washed with ethanol several times, and then dried in air at 80

°C for 12 h. The samples are also prepared with various concentrations of Ni and adscititious H_2O at 170 °C for 6 h.

The samples prepared with 0.14 M Ni for 6 h were treated with various concentration of KOH. In a typical procedure, the sample (0.2 g) was added into 20 ml KOH solution to get a suspension. The suspension was stirred for 30 min at room temperature and then kept for another 24 hours. The solid products were collected by centrifugation, washed with ethanol several times, and then dried in air at 80 °C for 12 h. The samples prepared with 0.14 M Ni for 6 h were also heated at various temperature for 3 h in air. The solid products were collected for further analysis.

2.2. Characterization

Powder X-ray diffraction (XRD) was used to characterize the samples. Data were collected on a X'Pert PRO X-ray diffractometer with Cu Kα radiation (λ=1.54178 Å) at a beam current of 40 mA. The morphologies of the samples were investigated by using a Hitachi S-4800 field-emission scanning electron microscope (FE-SEM) with cold field emitter. Transmission electron microscopy (TEM) and high resolution transmission electron microscopy (HRTEM) were used to verify the morphology and investigate the crystallographic characteristics of the samples. TEM studies were carried out on a Philips CM200 with accelerating voltage of 160 kV. HRTEM studies were carried out on a Tecnai F20 with accelerating voltage of 200 kV. Infrared spectra were collected with a resolution of 2 cm^{-1} by a fourier transform infrared spectrometer (Nicolet 5700). Energy dispersive X-ray analysis (EDX) was carried out on a Hitachi S-3400 with the attachment. Raman spectra were collected using Labor Raman HR-800 (France, Gobrnyron) and the 514 nm line of a He–Cd laser. UV-vis optical absorption spectra were collected using TU-1901 spectrometer (Puxi, China).

2.3. Electrochemical characterization

The nickel hydroxide powder was mixed with black carbon and polytetrafluoroethylene (PTFE) as a binder in a weight ratio of 80:10:10. Then the mixture was coated on a glassy carbon (GC) disk electrode. The pasted nickel electrodes were dried at 60 °C. The cyclic voltammetry (CV) measurements were carried out on an electrochemical workstation (CHI1140A, Chenhua, China). The experiments were carried out in a three-electrode glass cell in which contained the nickel electrode as the working electrode, Pt wire as the counter electrode, Hg/HgO as the reference electrode, and 6 M KOH aqueous solution as the electrolyte.

2.4 Wastewater treatment evaluation

In this experiment, acid fuchsine was used as organic pollutants, and the samples prepared with 2 M KOH and 6 M KOH were used as adsorbents. Acid fuchsine (6 mg/L, 100mL) was mixed with the adsorbent (50 mg) under stirring. The suspension was taken from the bottle at given time intervals. The clear solution was obtained after removing the sample from the suspension by centrifugation. The adsorption process was monitored by a UV-vis spectrophotometer (TU-1901, Puxi).

3. Results and discussion

3.1. Effects of reaction time on the crystallinity and morphology

Fig. 1 shows XRD patterns of the samples prepared for various time. In Fig. 1, the peaks located at 15.5°, 33°, 55.9° and 58.2° are corresponding to the d-spacing of 5.71 Å, 2.73 Å, 1.64 Å and 1.58 Å, respectively. Feitknecht et al.[14] reported that the NiCl(OH) has a hexagonal unit cell with a=3.25 Å, c=34.01 Å, Z=6. Hu et al.[15] reported that XRD pattern of the nickel

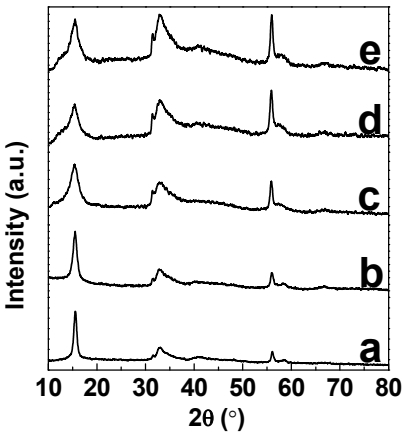

Figure 1. XRD patterns of the samples prepared for various time: (a) 3 h, (b) 4 h, (c) 6 h, (d) 12 h, (e) 18 h.

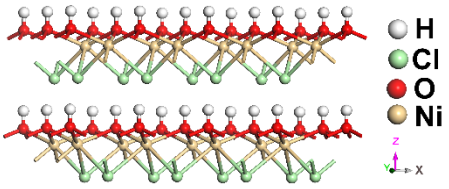

Figure 2. Schematic diagram of the crystal structure of nickel hydroxychloride.

hydroxychloride fullerene-like colloidal nanocrystal fabricated in oleic acid-oleylamine mixture with a colloidal synthetic route shows a strong peak at 15.7°, an asymmetry peak in the 30°-40° region and a peak at 58.2°. By comparing Fig. 1 with the XRD results reported by Feitknecht et al. and Hu et al., the samples are suggested to be nickel hydroxychloride. Fig. 2 shows schematic diagram of the crystal structure of nickel hydroxychloride. Nickel hydroxychloride, which is built up from neutral layers of $[Ni(OH)_{3/3}Cl_{3/3}]$-octahedra, has the hexagonal structure of Cd(OH)Cl[16]. The nickel atoms are in the octahedral sites defined by three chlorine atoms on one side and three hydroxyls groups on the other side.

By the calculation of the peaks at 15.5° using Scherrer equation, the crystal sizes of the samples prepared for 3 h, 4 h, 6 h, 12 h and 18 h are 11.5 nm, 7.7 nm, 4.0 nm, 3.3 nm, 3.2 nm, respectively, indicating that the crystal sizes of the samples decrease in c-axis direction as the reaction time increases. By the calculation of the peaks at 55.9° using Scherrer equation, the crystal sizes of the samples prepared for 3 h, 4 h, 6 h, 12 h and 18 h are 17.2 nm, 15.6 nm, 15.9 nm, 15.9 nm, 15.6 nm, respectively, indicating that the crystal sizes of the samples have no significant change in a-axis direction as the reaction time increases. Therefore, it is suggested that a preferred dissolution of nickel hydroxychloride may occur in the c-axis direction as the reaction time increases. In 30°-40° region, the pronounced asymmetry peaks are observed due to a turbostratic characteristic of brucite-like structures arising from the rotation of the layers and the loss of registry among successive layers[6, 17, 18]. In the present work, as the reaction time increases, the intensity of the peaks in 30°-40° region increases, suggesting that the structural ordering of the nickel hydroxychloride layers decreases as the reaction time increases.

Fig. 3 shows FE-SEM images of the samples prepared for various time. In Fig. 3a and Fig. 3b, the aggregated microspheres are obtained for 3 h. The microspheres are

composed of thick sheets and particles (see Fig. 3b). In Fig. 3c and Fig. 3d, the irregular microspheres composed of crumpled nanosheets are obtained for 4 h. In Fig. 3e and Fig. 3f, well-defined microspheres are obtained for 6 h and the microspheres are composed of crumpled nanosheets with random orientation. FE-SEM images of the samples prepared for 9 h, 12 h and 18 h show that the flower-like microspheres are also obtained (see Fig. S1).

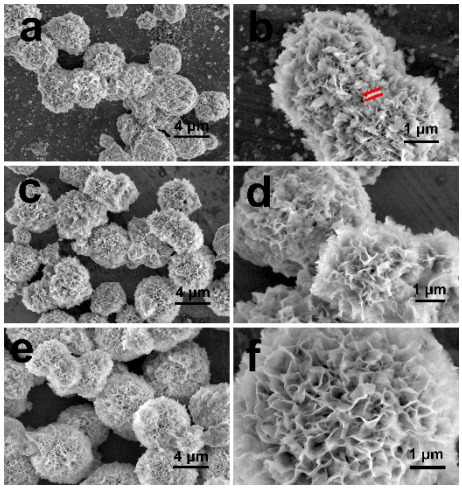

Figure 3. FE-SEM images of the samples prepared for various time: (a and b) 3 h, (c and d) 4 h, (e and f) 6 h.

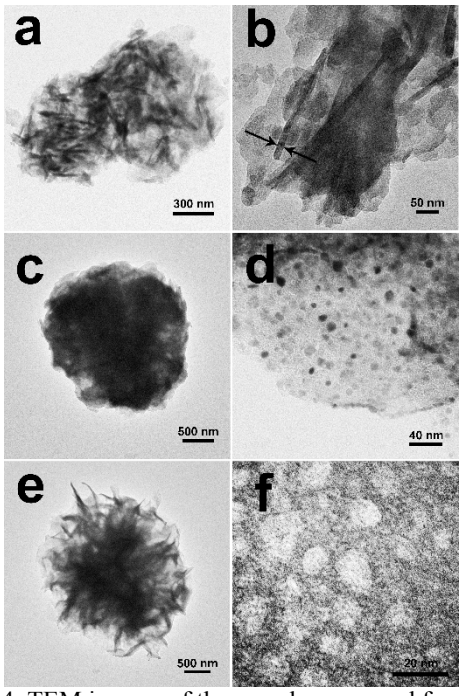

Figure 4. TEM images of the samples prepared for various time: (a and b) 3 h, (c and d) 4 h, (e and f) 9 h.

Fig. 4 shows TEM images of the samples prepared for various time. Fig. 4a shows that the microspheres prepared for 3 h are composed of rigid nanosheets, which is consistent with FE-SEM result (see Fig. 3a-b). Fig. 4b shows that the thickness of the nanosheets is about 20 nm which is estimated by the width of the high-contrast section. Fig. 4c shows that the irregular spherical shaped microsphere is prepared for 4 h. Fig. 4d shows that the nanosheet of the microsphere is consisted of nanoparticles. Fig. 5 shows TEM images, SAED pattern and HRTEM image of the sample prepared for 6 h. Fig. 5a shows that well-defined microspheres are obtained and the microspheres are composed of crumpled nanosheets. Fig. 5b shows that a lot of pores are distributed in the nanosheets. According to the SAED pattern (see Fig. 5c), the sample is nickel hydroxychloride with moderate crystallinity. Fig. 5d shows that the weak visible lattice fringes are observed and the crystal size is about 4 nm, indicating that the nanosheets are composed of nanoparticles with moderate crystallinity. Fig. 4e shows that the flower-like microsphere with crumpled nanosheets is prepared for 9h. Fig. 4f shows that there are a lot of pores about 10 nm in the nanosheet.

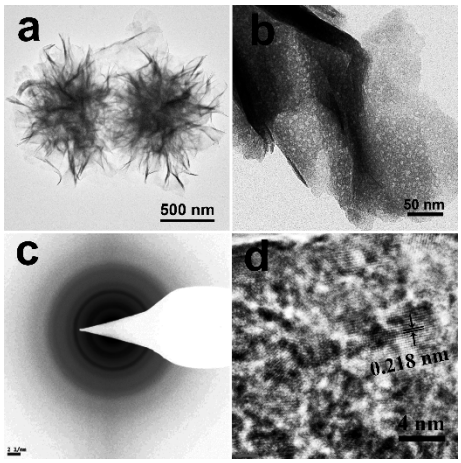

Figure 5. TEM images (a and b), SAED pattern (c) and HRTEM image (d) of the sample prepared for 6 h.

Fig. 6a-c show EDX pattern, UV-vis spectrum and Raman spectrum of the sample prepared for 6 h, respectively. According to EDX pattern (see Fig. 6a), the atom ratio of O, Cl and Ni is close to 1:1:1 in the sample. UV-vis optical absorption spectrum reveals that a steep absorption edge observed at 377 nm is attributed to band gap absorption (see Fig. 6b). The band gap (E_g) can be obtained from the equation E_g (eV) = 1240/λ (nm), where λ is the onset value of absorption edge[19]. Therefore, the band gap of the sample is about 3.29 eV. The absorption spectrum exhibits other two broad bands at about 424 nm and 530 nm, which are attributed to d–d transitions of Ni compounds within the band gap. Raman spectrum (Fig. 6c) reveals that the peak at 776 cm^{-1} is assigned to a librational mode of the hydroxyl and the peaks at 464, 403, 246, 219, 166, 123 cm^{-1} are suggested to be assigned to lattice vibrations modes[20]. However, the assignments of the Raman active modes to the peaks below 500 cm^{-1} are presently uncertain.

Fig. 6d shows FT-IR spectra of the samples prepared for 3 h, 6 h and 18 h. In Fig. 6d, four peaks (the sharp peaks at 3561 and 754 cm^{-1}, the board peaks at 3376 and 1620 cm^{-1}) are observed. The strong absorption peaks at 3561 cm^{-1} are attributed to the ν_{O-H} stretching vibration[15], which confirms the brucite-like structure of nickel hydroxychloride. The sample prepared for 18 h has stronger ν_{O-H} stretching vibration at 3561 cm^{-1} than those prepared for 3 h and 6 h. The broad peaks at 3376 cm^{-1} are due to the ν_{O-H} vibration of hydrogen-bonded hydroxyl groups[18]. The peaks at 1620 cm^{-1} are due to δ_{H2O} vibration of the water molecule adsorbed in the sample. In the

low wavenumber (800-400 cm^{-1}) region, the strong peaks at 754 cm^{-1} are assigned to $\delta_{(Ni\text{-}O\text{-}H)}$ vibration[6, 21].

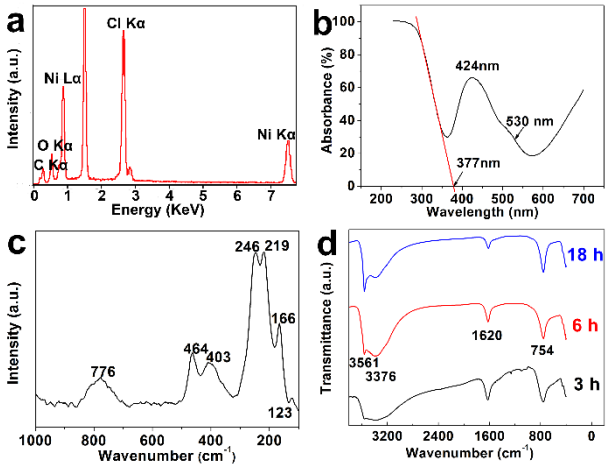

Figure 6. EDX pattern (a), UV-vis spectrum (b) and Raman spectrum (c) of the sample prepared for 6 h. (d) FT-IR spectra of the samples prepared for 3 h, 6 h and 18 h.

3.2. Effects of H_2O on the crystallinity and morphology

Fig. 7 shows XRD patterns of the samples prepared with various amount of H_2O. The samples are also nickel hydroxychloride. As the amount of H_2O increases, the crystallinity of the samples is significantly improved. It is noteworthy that XRD pattern of the sample prepared with 5.1 M H_2O doesn't show turbostratic characteristic in the 30°-40° region (see the curve c), and the diffraction peaks are indexed using the crystallographic data obtained from Feitknecht[14]. X-ray diffraction powder data of the sample prepared with 5.1 M H_2O are listed in Tab. S1.

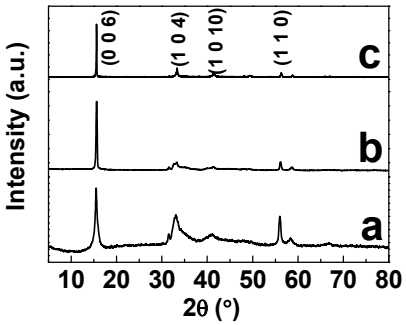

Figure 7. XRD patterns of the samples prepared with various amount of H_2O: (a) 0.85 M, (b) 1.7 M, (c) 5.1 M.

Fig. 8a-c show FE-SEM images of the samples prepared with various amount of H_2O. The flower-like microspheres and the platelet structures are prepared with 0.85 M H_2O and 1.7 M H_2O (see Fig. 8a and Fig. 8b), while irregular structures composed of rigid nanosheets are prepared with 5.1 M H_2O (see Fig. 8c). Fig. 8d-f show TEM images and the corresponding SAED pattern of the sample prepared with 0.85 M H_2O. The flower-like microspheres composed of rigid nanosheets (see Fig. 8d) and the platelet structures (see Fig. 8e) are observed. The platelet structures show hexagonal single-crystal characteristic (see Fig. 8f).

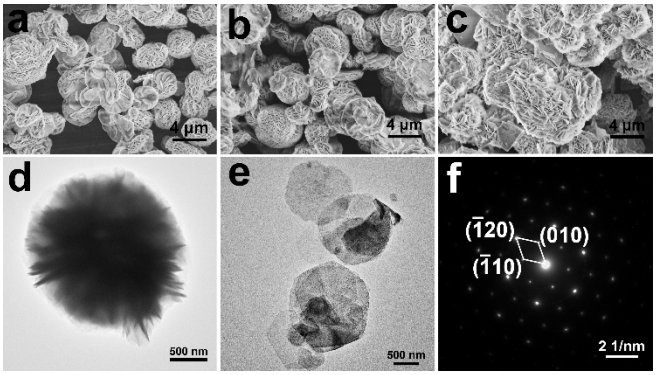

Figure 8. FE-SEM images of the samples prepared with various amount of H_2O: (a) 0.85 M, (b) 1.7 M, (c) 5.1 M. TEM images (d and e) and the corresponding SAED pattern (f) of the sample prepared with 0.85 M H_2O.

3.3. Effects of Ni concentration on the crystallinity and morphology

Fig. 9 shows XRD patterns of the samples prepared with various concentration of Ni. The sample prepared with 0.014 M Ni has quite low crystallinity (see the curve a), while the samples prepared with 0.035 M and 0.21 M Ni have good crystallinity (see the curve b-c), indicating that higher crystallinity can be obtained when the sample is prepared with higher concentration of Ni. Fig. 10a-d show FE-SEM images of the samples prepared with various concentration of Ni. The flower-like microspheres are prepared with 0.014 M and 0.07 M Ni (see Fig. 10a and Fig. 10b). The microspheres composed of thick sheets and particles are prepared with 0.21 M Ni (see Fig. 10c). However, the platelet structures are prepared with 0.35 M Ni (see Fig. 10d). TEM image and corresponding SAED pattern of the sample prepared with 0.35 M Ni reveal that the platelet structure shows hexagonal single-crystal characteristic (see Fig. 10e-f).

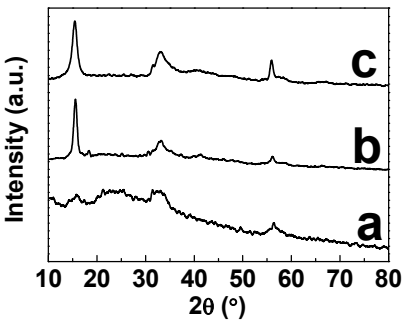

Figure 9. XRD patterns of the samples prepared with various concentration of Ni: (a) 0.014 M, (b) 0.07 M, (c) 0.21 M.

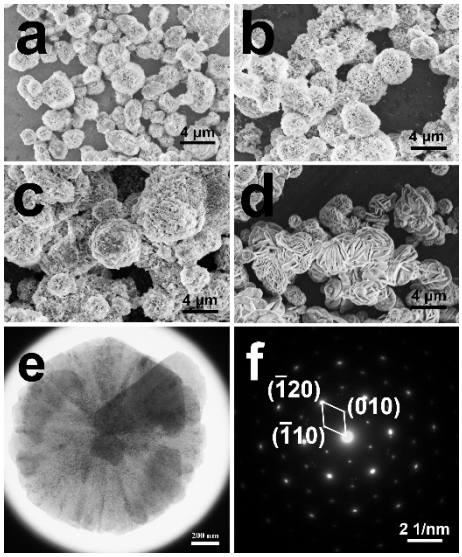

Figure 10. FE-SEM images of the samples prepared with various concentration of Ni: (a) 0.014 M, (b) 0.07 M, (c) 0.21 M, (d) 0.35 M. TEM image (e) and the corresponding SAED pattern (f) of the sample prepared with 0.35 M Ni.

3.4. Effects of KOH concentration on crystallinity and morphology

Fig. 11 shows XRD patterns of the samples prepared by nickel hydroxychloride microspheres treated with various concentration of KOH. In the curve a, except the broad peak around 17°, the diffraction peaks are assigned to β-$Ni(OH)_2$ (JCPDS No. 14-0117). In the curve b-c, all the diffraction peaks of the samples prepared with 2 M and 6 M KOH are assigned to β-$Ni(OH)_2$, indicating that pure β-$Ni(OH)_2$ is prepared by nickel hydroxychloride microspheres treated with high concentration of KOH.

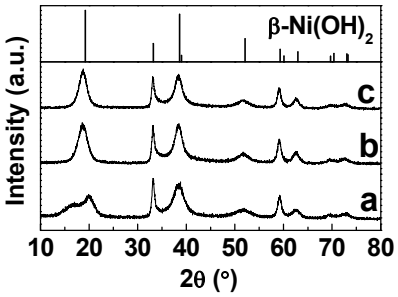

Figure 11. XRD patterns of the samples prepared by nickel hydroxychloride microspheres treated with various concentration of KOH: (a) 0.1 M, (b) 2 M, (c) 6 M.

Due to the similar crystal structures between nickel hydroxychloride and β-$Ni(OH)_2$, the crystal sizes of the samples before and after the treatment could be compared. By the calculation of the peaks at 19.2° using Scherrer equation, the crystal sizes of the samples prepared with 2 M and 6 M KOH are about 4 nm. By the calculation of the peaks at 33.2° and 59.3° using Scherrer equation, the crystal sizes of the samples prepared with 2 M and 6 M KOH are about 10 nm. On the other hand, the crystal size of nickel hydroxychloride before the treatment is about 4 nm in the c-axis direction and 15.9 nm in the a-axis direction (see Fig. 1c). It suggests that the crystal sizes of the samples don't change obviously in the c-axis direction but decrease in a-axis direction during the treatment with KOH.

Fig. 12 shows FE-SEM images of the samples prepared by nickel hydroxychloride microspheres treated with various concentration of KOH. Fig. 12a shows that irregular flower-like microspheres are prepared with 0.1 M KOH. Fig. 12b shows that the microspheres are composed of nanosheets with lots of defects. Fig. 12c and Fig. 12d show that well-defined microspheres are prepared with 2 M and 6 M KOH, but the nanosheets of the microspheres also have some defects. According to Fig. 12, the flower-like β-$Ni(OH)_2$ microspheres are prepared by nickel hydroxychloride microspheres treated with high concentration of KOH.

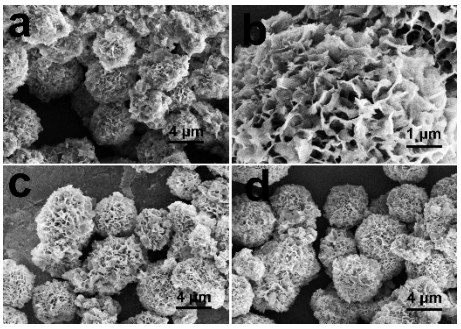

Figure 12. FE-SEM images of the samples prepared by nickel hydroxychloride microspheres treated with various concentration of KOH: (a and b) 0.1 M, (c) 2 M, (d) 6 M.

FE-SEM image of the sample prepared by nickel hydroxychloride microspheres after heat treatment at 350 °C shows that the flower-like structures are destroyed and the particles are prepared under the heat treatment (see Fig. S2). XRD patterns of the sample prepared by nickel hydroxychloride microspheres after heat treatment at various temperature show that pure NiO (JCPDS: No. 22-1189) is prepared when the temperature is 350 °C or higher (see Fig. S3). The crystal size of the sample obtained from the Scherrer equation is about 44 nm when the heat treatment temperature is 350 °C. As the temperature increases from 350 °C to 750 °C, the crystal size of the samples increases from 44 nm to 53 nm (see Fig. S4).

3.5. The formation mechanisms of the flower-like nickel hydroxychloride microspheres and β-$Ni(OH)_2$ microspheres

According to the above discussion, well-defined flower-like microspheres are prepared with low concentration of Ni without adding H_2O. Fig. 13 shows schematic diagram of the formation process of the flower-like nickel hydroxychloride microspheres and β-$Ni(OH)_2$ microspheres. The nickel hydroxychloride is suggested to be produced by the forced hydrolysis of $NiCl_2 \cdot 6H_2O$ in the solvothermal process. The formation process of the nickel hydroxychloride microspheres may be divided into several steps. Firstly, the forced hydrolysis occurs and the nucleation of nickel hydroxychloride happens. Secondly, the condensation and the aggregation growth of nickel hydroxychloride occur, which produces nickel hydroxychloride microspheres composed of thick sheets and particles (see Fig. 3a-b and Fig. 4a-b). As the reaction proceeds, a dissolution-recrystallization process happens within the microspheres. Then the flower-like nickel hydroxychloride microspheres composed of crumpled nanosheets are formed (see Fig. 4e and Fig. 5). Finally, the flower-like β-$Ni(OH)_2$

microspheres are prepared by nickel hydroxychloride microspheres treated with high concentration of KOH (see Fig. 12).

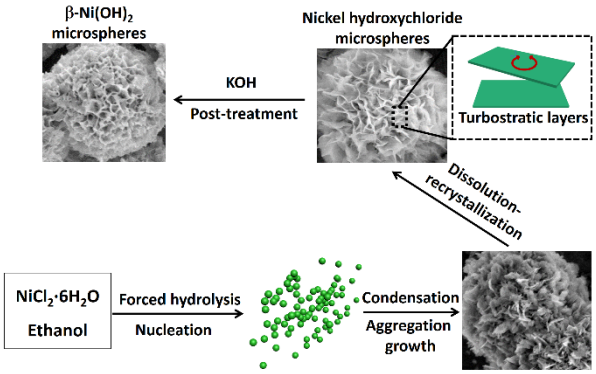

Figure 13. Schematic diagram of the formation process of the flower-like nickel hydroxychloride microspheres and β-$Ni(OH)_2$ microspheres.

When the sample is prepared with H_2O, the nucleation and growth rates of nickel hydroxychloride increase because the forced hydrolysis is promoted. Moreover, the arrangement of nickel hydroxychloride layers may be adjusted by H_2O through H-bonding, leading to the decrease of turbostratic characteristic of the samples (see. Fig. 7). Therefore, the ordered stacking of the nickel hydroxychloride layers occurs and the dissolution-recrystallization process may be suppressed, which leads to the formation of platelet structures or the rigid nanosheets (see Fig. 8). When the sample is prepared with high concentration of Ni, the nucleation and growth rates of nickel hydroxychloride also increase and the continued crystal growth of nickel hydroxychloride is favorable in this situation, which leads to the formation of the platelet structures (see Fig. 10d).

β-$Ni(OH)_2$ is prepared by the replacement of Ni-Cl bonding of nickel hydroxychloride with Ni-OH bonding. Though nickel hydroxychloride has similar crystal structure with β-$Ni(OH)_2$, the decrease of the interlayer distance occurs during the transformation. Moreover, the nickel hydroxychloride layers within the flower-like structures show remarkably turbostratic characteristic (see Fig. 1c), while the β-$Ni(OH)_2$ layers within the flower-like structures don't show such characteristic (see Fig. 11). It suggests that great structural adjustment within the nanosheets and the microspheres may occur during the transformation. When the flower-like nickel hydroxychloride microspheres are treated with low concentration of KOH, the low transformation rate of nickel hydroxychloride may cause great stress within the nanosheets and the microspheres. Therefore, the structural collapse of the flower-like microspheres occurs during the transformation, leading to the formation of irregular structures (see Fig. 12a-b). When the flower-like nickel hydroxychloride microspheres are treated with high concentration of KOH, the chlorine atoms in the same layers are almost replaced simultaneously and the structural adjustment of the layers is facilitated, leading to the formation of the flower-like microspheres with better structural integrity.

3.6. Electrochemical performance of β-$Ni(OH)_2$

Fig. 14 shows cyclic voltammograms of the samples prepared by nickel hydroxychloride microspheres treated with 2 M KOH and 6 M KOH at a scan rate of 10 mV s^{-1}. As shown in Fig. 14, the strong terminal peaks deal with the oxidation peaks of water. For cyclic voltammogram of the sample prepared with 2 M KOH, one anodic oxidation peak appears at about 290 mV, which is associated with the over-oxidation of β-$Ni(OH)_2$ to γ-NiOOH by intensive oxygen evolution on the electrode[22]. Another anodic oxidation peak, partially overlapped with the oxygen evolution peak, appears at 400-500 mV, which is associated with the conversion of β-$Ni(OH)_2$ to β-NiOOH[23]. The reduction peak appearing at about 195 mV is associated with the conversion of oxyhydroxide back to nickel hydroxide[24]. For cyclic voltammogram of the sample prepared with 6 M KOH, only one anodic oxidation peak at about 400 mV and one oxyhydroxide reduction peak at about 197 mV are observed, which is associated with the conversion between β-$Ni(OH)_2$ and β-NiOOH. The formation of γ-NiOOH leads to the volume expansion of the nickel hydroxide electrode, which affects the effective contact among particles of active materials and limits the electrochemical performance of nickel hydroxide electrodes[25]. Moreover, the oxygen evolution reaction (OER) is known as a parasitic reaction during the charge process, which also limits the electrochemical performance of nickel hydroxide electrodes. As shown in Fig. 14, the separation between the oxidation peak potential and the OER potential for the sample prepared with 2 M KOH is smaller than that for the sample prepared with 6 M KOH, suggesting that the sample prepared with 6 M KOH shows better electrochemical performance. This may be because β-$Ni(OH)_2$ microspheres prepared with higher concentration of KOH have better structural integrity.

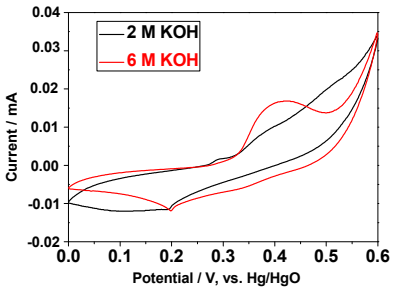

Figure 14. Cyclic voltammograms of the samples prepared by nickel hydroxychloride microspheres treated with 2 M KOH and 6 M KOH at a scan rate of 10 mV s^{-1}.

3.7 Adsorption activity of β-$Ni(OH)_2$

Fig. 15a shows the molecular structure of acid fuchsine. Acid fuchsine, a typical anionic dye, is mainly used for biological staining and tissue staining. Due to its stable structure, it is difficult to degrade acid fuchsine in wastewater through traditional chemical and biological approaches. Fig. 15b-c show UV-vis absorption spectra of acid fuchsine solution in the presence of the samples prepared by nickel hydroxychloride microspheres treated with 2 M KOH and 6 M KOH. The intensity of the absorption peaks at 524 nm gradually decreases as the absorption time increases (see Fig. 15b-c). Fig. 15d show the degradation profiles of acid fuchsine in the presence of the samples prepared by nickel hydroxychloride microspheres treated with 2 M KOH and 6 M KOH as adsorbents. The adsorption rates within the first 5 min were very fast, which may be attributed to the unique structures of the flower-like β-$Ni(OH)_2$ microspheres. It can be seen that the sample prepared with 2 M KOH has higher adsorption rate. In 80 min, the sample prepared with 2 M KOH could remove about 90% of the acid fuchsine, while the sample prepared with

6 M KOH could remove about 75% of the acid fuchsine, indicating that the sample prepared with 2 M has greater adsorption capacity. According to Fig. 15d, the sample prepared with 2 M KOH has obviously better ability to adsorb acid fuchsine than the sample prepared with 6 M KOH. This may be because the sample prepared with 2 M KOH has more defects which serve as active sites for the adsorption of acid fuchsine.

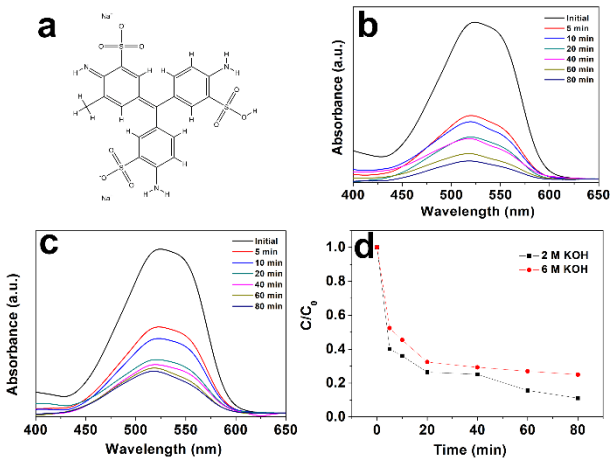

Figure 15. The molecular structure of acid fuchsine (a); UV-vis absorption spectra of acid fuchsine solution in the presence of the samples prepared by nickel hydroxychloride microspheres treated with (b) 2 M KOH and (c) 6 M KOH; the degradation profiles of acid fuchsine in the presence of the samples prepared by nickel hydroxychloride microspheres treated with 2 M KOH and 6 M KOH as adsorbents (d).

Conclusions

Hierarchical flower-like nickel hydroxychloride microspheres are successfully synthesized via a template-free solvothermal method, involving aggregation growth and dissolution-recrystallization process. The flower-like nickel hydroxychloride microspheres composed of crumpled nanosheets are prepared with low concentration of Ni without adding H_2O, while the platelet structures are prepared with high concentration of Ni or by adding appropriate amount of H_2O. The flower-like β-$Ni(OH)_2$ microspheres are prepared by nickel hydroxychloride microspheres treated with high concentration of KOH. The β-$Ni(OH)_2$ microspheres prepared with higher concentration of KOH show better electrochemical performance, while the β-$Ni(OH)_2$ microspheres prepared with lower concentration of KOH show better adsorption activity for acid fuchsine.

Acknowledgements

This research is supported by the National Natural Science Foundation (Grant No. 51172201), Key Science and Technology Innovation Team of Zhejiang Province (Grant No. 2010R50013) and Key Technologies R&D Program of China (2013BAE03B00).

Notes and references

† State Key Laboratory of Silicon Materials and Department of Materials Science and Engineering and Key Laboratory of Advanced Materials and Applications for Batteries of Zhejiang Province, Zhejiang University, Hangzhou 310027, P. R. China.
Tel: 86-571-87952341; Email: glzhao@zju.edu.cn.

Electronic Supplementary Information (ESI) available: [details of any supplementary information available should be included here]. See DOI: 10.1039/b000000x/

1. I. Lisiecki, *J. Phys. Chem. B*, 2005, **109**, 12231.
2. P. Li, D. Wang, Q. Peng and Y. Li, *Cryst. Growth Des.*, 2013, **13**, 1949.
3. G. Centi and S. Perathoner, *Micropor. Mesopor. Mater.*, 2008, **107**, 3.
4. Y. Cudennec, A. Riou, Y. Gérault and A. Lecerf, *J. Solid State Chem.* , 2000, **151**, 308.
5. B. Weckler and H. D. Lutz, *Spectrochim. Acta, Part A* 1996, **52**, 1507.
6. M. Rajamathi and P. Vishnu Kamath, *J. Power Sources* 1998, **70**, 118.
7. J. Tian, Z. Xing, Q. Chu, Q. Liu, A. M. Asiri, A. H. Qusti, A. O. Al-Youbi and X. Sun, *CrystEngComm*, 2013, **15**, 8300.
8. H. B. Li, P. Liu, Y. Liang, J. Xiao and G. W. Yang, *CrystEngComm*, 2013, **15**, 4054.
9. S. Ran, Y. Zhu, H. Huang, B. Liang, J. Xu, B. Liu, J. Zhang, Z. Xie, Z. Wang, J. Ye, D. Chen and G. Shen, *CrystEngComm*, 2012, **14**, 3063.
10. L.-P. Zhu, G.-H. Liao, Y. Yang, H.-M. Xiao, J.-F. Wang and S.-Y. Fu, *Nanoscale Res. Lett.* , 2009, **4**, 550.
11. Q. Y. Li, R. N. Wang, Z. R. Nie, Q. Wei and Z. H. Wang, *J. Alloys Compd.* , 2010, **496**, 300.
12. S. Ran, Y. Zhu, H. Huang, B. Liang, J. Xu, B. Liu, J. Zhang, Z. Xie, Z. Wang and J. Ye, *CrystEngComm*, 2012, **14**, 3063.
13. Y. Luo, G. Duan and G. Li, *J. Solid State Chem.* , 2007, **180**, 2149.
14. H. R. Oswald and W. Feitknecht, *Helv. Chim. Acta* 1961, **44**, 847.
15. S. Hu and X. Wang, *J. Am. Chem. Soc.* , 2010, **132**, 9573.
16. Y. Cudennec, A. Riou, Y. Gerault and A. Lecerf, *J. Solid State Chem.* , 2000, **151**, 308.
17. T. N. Ramesh, M. Rajamathi and P. V. Kamath, *Solid State Sci.* , 2003, **5**, 751.
18. G. J. d. A. A. Soler-Illia, M. Jobbágy, A. E. Regazzoni and M. A. Blesa, *Chem. Mater.* , 1999, **11**, 3140.
19. A. Kudo and Y. Miseki, *Chem. Soc. Rev.* , 2009, **38**, 253.
20. S. R. Shieh and T. S. Duffy, *Phys. Rev. B*, 2002, **66**, 134301.
21. P. Oliva, J. Leonardi, J. F. Laurent, C. Delmas, J. J. Braconnier, M. Figlarz, F. Fievet and A. d. Guibert, *J. Power Sources* 1982, **8**, 229.
22. H. Zhou and Z. Zhou, *Solid State Ionics* 2005, **176**, 1909.
23. B. Li, H. Cao, J. Shao, H. Zheng, Y. Lu, J. Yin and M. Qu, *Chem. Commun.* , 2011, **47**, 3159.
24. W. Zhou, M. Yao, L. Guo, Y. Li, J. Li and S. Yang, *J. Am. Chem. Soc.* , 2009, **131**, 2959.
25. L.-X. Yang, Y.-J. Zhu, H. Tong, Z.-H. Liang and W.-W. Wang, *Crystal Growth and Design*, 2007, **7**, 2716.